Available online at www.sciencedirect.com
SCIENCE @ DIRECT®
ELSEVIER
Journal of the European Ceramic Society 25 (2005) 2363–2368
JECS
www.elsevier.com/locate/jeurceramsoc

The LIMM problem for ferroelectric thin films comprising space charge layers

G. Suchaneck [a,*], A.V. Solnyshkin [b], D.A. Kiselev [b], A.A. Bogomolov [b], G. Gerlach [a]

[a] *Dresden University of Technology, Institute for Solid State Electronics, Mommsenstr. 13, 01062 Dresden, Germany*
[b] *Tver State University, Department of Ferroelectric and Piezoelectric Physics, Sadovij per., 35, 170002 Tver, Russia*

Available online 25 March 2005

Abstract

In this work, the laser intensity modulation method (LIMM) problem is reconsidered for the generalized case of a multilayer structure consisting of layers with ferroelectric polarization, with both ferroelectric and space charge induced polarization, and with solely space charge induced polarization. Usually, the problem reduces to the calculation of the internal electric field. Boundary conditions are derived from the electric displacement of a short-circuited structure. The calculations were compared with the pyroelectric spectrum of PZT thin films of different thickness and a model metal–ferroelectric–semiconductor structure consisting of Pt–ferroelectric PZT (perovskite)–semiconducting PZT (fluorite).
© 2005 Elsevier Ltd. All rights reserved.

Keywords: Ferroelectric properties; PZT; Perovskites; Pyroelectric spectroscopy

1. Introduction

The laser intensity modulation method (LIMM) was developed in the 1980s of the last century by Lang and Das-Gupta[1] as an extension of Collin's temperature pulse method[2] and Chynoweth's technique for dynamic pyroelectric measurements.[3] A similar to LIMM approach was first proposed by Bezdetny et al.[4] They considered a lossy ferroelectric, derived a Fredholm integral equation similar to that of the LIMM problem, and used sinusoidally modulated noncoherent light at frequencies up to 1 kHz for measurement.

LIMM determines the spatial polarization profile from the pyroelectric current spectrum caused by the interaction of a thermal wave generated by an intensity modulated laser and the unknown polarization distribution. If the incoming laser light is modulated with a circular frequency ω, the complex pyroelectric current yields to[5]

$$I(\omega, t) = I_{\mathrm{p}} \mathrm{e}^{\mathrm{j}\omega t} = \frac{A_{\mathrm{S}}}{d} \int_0^d r(z) \frac{\partial}{\partial t} \hat{\underline{T}}(\omega, z, t)\, \mathrm{d}z, \tag{1}$$

where I_{p} is the complex amplitude of the pyroelectric current, z the depth coordinate, t the time, $\hat{\underline{T}}$ the complex amplitude of the temperature, A_{S} the heated area of the sample, d the ferroelectric film thickness, $r(z)$ the response function. The pyroelectric response function

$$r(z) = p(z) - (\alpha_z - \alpha_\varepsilon)\varepsilon\varepsilon_0 E_{\mathrm{int}}(z), \tag{2}$$

is determined both by the pyroelectric coefficient $p(z)$ and the internal electric field E_{int}. This internal field is generated in a short-circuited sample ($E = 0$ at electrode surfaces) by the presence of space charges and the depolarization field,

$$E_{\mathrm{int}}(z) = \frac{1}{\varepsilon\varepsilon_0} \left[\left(\int_0^z \rho(\zeta)\, \mathrm{d}\zeta - \frac{1}{d} \int_0^l \left(\int_0^{z'} \rho(\zeta)\, \mathrm{d}\zeta \right) \mathrm{d}z' \right) - \left(P(z) - \frac{1}{d} \int_0^l P(z')\, \mathrm{d}z' \right) \right] = \delta E_{\mathrm{sc}} - \frac{\delta P}{\varepsilon\varepsilon_0}, \tag{3}$$

* Corresponding author. Tel.: +49 351 463 5281; fax: +49 351 463 2320.
E-mail address: suchanec@rcs.urz.tu-dresden.de (G. Suchaneck).

0955-2219/$ – see front matter © 2005 Elsevier Ltd. All rights reserved.
doi:10.1016/j.jeurceramsoc.2005.03.057

where α_z is the relative thermal expansion coefficient, α_ε the relative temperature coefficient of the dielectric constant, ε the dielectric constant, $P(z)$ the spatially dependent spontaneous polarization, and $\rho(z)$ the spatially dependent space charge density. Without a priory knowledge of the space charge distribution, a separation of the pyroelectric response and the space charge distribution is not possible by using LIMM alone.[6] Thus, the internal electric field $E_{\mathrm{int}}(z)$ must be determined separately.

Usually, the pyroelectric spectrum is analyzed assuming a local compensation of the polarization gradient by an appropriate charge density $\rho = \mathrm{d}P/\mathrm{d}z$.[5,7,8] According to Eq. (3), this leads to the simple case $E_{\mathrm{int}} = 0$ and consequently $r(z) = p(z)$. However,

- (i) the existence of space charge layers at the surface of ferroelectric crystals is known for half a century,[9]
- (ii) a depolarization field always occurs in thin insulating ferroelectric films due to the existence of a finite separation between the polarization charge and the compensating free charge,[10] if a gradient in the polarization exists over some appreciable distance near the electrode interface, if the compensating charge in the electrodes is distributed over a finite screening distance, or especially if there are nonswitching layers in the ferroelectric film near the interfaces,
- (iii) a space charge layer is artificially introduced during the initial film growth to produce self-polarized elements of pyroelectric sensor arrays,[8]
- (iv) a space charge layer is formed at the metal electrode/ferroelectric interface which depends on the contact potential difference.[11]

The electric polarization in the ferroelectric layer causes also depletion or accumulation of carriers near the interface of heterostructures composed of ferroelectric and semiconducting, superconducting, or magnetoresistive perovskites. Such heterostructures are promising candidates to achieve electric-field tuned ferromagnetic metal–insulator, and superconductor–insulator phase transitions at room temperature. Moreover, due to the existence of a depolarization field, there is always a lack of compensation.

In this work, the LIMM problem is reconsidered for the generalized case of a multilayer structure consisting of layers with ferroelectric polarization, with both ferroelectric and space charge induced polarization, and with solely space charge induced polarization. The problem is reduced to the calculation of the internal electric field. Boundary conditions are derived from the electric displacement of a short-circuited structure. The calculations were compared with a model metal–ferroelectric–semiconductor structure consisting of Pt–ferroelectric PZT (perovskite)–semiconducting PZT (fluorite).

2. Theory

The pyroelectric coefficient of a thin film laterally perfectly clamped in the substrate plane is given by[12]

$$p_3 = p_3^T - \frac{2d_{31}\alpha_1}{s_{11} + s_{12}}, \tag{4}$$

where

$$p_3^T = p_3^S + \sum_j e_{3j}\alpha_j, \tag{5}$$

is the pyroelectric coefficient determined for uniform heating, constant mechanical stress T, and low electric field E, p^S the constant strain pyroelectric coefficient (called also primary pyroelectric coefficient), α_i the thermal expansion coefficients, s_{ij} are the elastic compliance constants, d_{ij} the piezoelectric strain constants, and e_{ji} the piezoelectric stress constants. Pyroelectric coefficients $p_3 = p(z)$ determined by LIMM for ferroelectric thin film on thin membranes are within the limits between the constant strain and the ideal clamping cases. They should be discussed individually.

The dielectric constant of ferroelectrics depends both on frequency and applied electric field. Therefore, the temperature dependence of the dielectric constant in Eq. (2) should be determined in a suitable way. Although there is an inherent relation between large-signal parameters (hysteresis) and small signal parameters (dielectric constant), the small-signal dielectric constant is not mere differential polarization and electric field change. By the application of small ac fields, the domain walls within the crystallite remain freely moveable, and they perform wall oscillations on a microscopic scale giving rise to an extrinsic contribution to dielectric properties. The relative temperature coefficient of the dielectric constant α_ε in Eq. (2) is related to the small signal value of an unbiased sample.[13] Recently, we could show that in special cases related to ferroelectrics comprising space charge layers, for instance self-polarized PZT thin films deposited by reactive sputtering, the extrinsic contributions to piezoelectric and dielectric properties are small.[14] In this case, the domain wall motion is negligible because of the domains are “locked” by space charges compensating the depolarization field at domain boundaries. However, domain wall oscillations are still present. For charge injection across interfaces the optical permittivity should be used since the injected electrons or holes are hot carriers, their transition time is too short to cause ionic and domain wall contributions to the dielectric constant.

The key issue of the LIMM problem for ferroelectric thin films comprising space charge layers is the calculation of the internal electric field E_{int} according to Eq. (3). As an example, we shall discuss a ferroelectric thin film with a nearly constant polarization distribution along the z-axis ($P(z) = P_s \approx \mathrm{const}$). The film has p-type conductivity due to cation vacancies that are formed by evaporation of a volatile during film deposition component, for instance PbO during PZT sputtering. In this case, the concentration of Pb vacancies is somewhat higher than that of O vacancies because of the corresponding

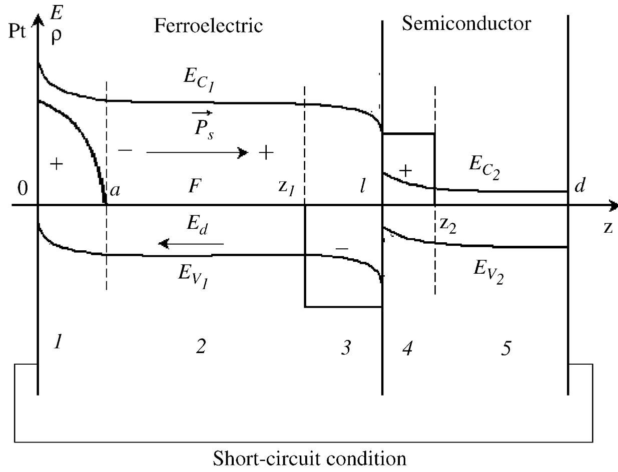

Fig. 1. Energy band diagram and space charge distribution of a metal–ferroelectric–semiconductor multilayer structure.

oxygen deficiency can be compensated to a certain extent by supplying oxygen from the air during cooling down.[15] The non-ferroelectric semiconductor is assumed to be of n-type conductivity (Fig. 1).

We consider short-circuit conditions ($E(0)=E(d)=0$) and take the potential distribution in region 1 as

$$\varphi_1(z) = \varphi_{1k}(z) + \varphi_d(z), \tag{6}$$

where $\varphi_{1k}(z)$ the potential distribution caused by the electrode/ferroelectric contact potential difference and where the electric potential of the depolarization field

$$\varphi_d(z) = A + bP_S z, \tag{7}$$

is dominated by the presence of a non-ferroelectric interface layer. Possible origins of the presence of a low-ε layer are size effects,[16] nonstoichiometric phases,[17] chemical reactions with the bottom electrode,[18] space charge layers,[19] electronic interface defects formed by charge carrier injection,[20] or film stress.[21] The depolarization field caused by the non-ferroelectric interface layer can be obtained from the additional tilting of the ferroelectric hysteresis loop and amounts to[22]

$$E_d = -\frac{d_i}{\varepsilon_i \varepsilon_0 d} P_S = -\frac{N}{\varepsilon_i \varepsilon_0} P_S = -bP_S, \tag{8}$$

where P_S is the ferroelectric spontaneous polarization, d_i the thickness of the non-ferroelectric boundary layer, and d the total thickness of the film. We assume $d_i \ll d$ and neglect for a moment the small changes of potential distribution introduced by the non-ferroelectric interface layer. This does not change the physical picture if we take into account the depolarization field according to Eq. (8), but makes the calculation less cumbersome. The boundary conditions of Eq. (6) are

$$\begin{cases} \varphi_1(0) = 0; \quad E_1 = -\left.\dfrac{d\varphi_1}{dz}\right|_{z=0} = 0 \\ \varphi_1(a) = -U_{1k} + A + bP_S a; \quad E_1 = -\left.\dfrac{d\varphi_1}{dz}\right|_{z=a} \\ = -bP = E_d \end{cases}. \tag{9}$$

The potential $\varphi_{1k}(z)$ is obtained by solving the Poisson's equation in the first region ($m=1$)

$$\frac{d^2\varphi_{mk}}{dz^2} = -\frac{\rho_m}{\varepsilon_m \varepsilon_0}, \tag{10}$$

for the following boundary conditions

$$\left.\frac{d\varphi_{1k}}{dz}\right|_{z=a} = 0; \quad \varphi_{1k}(a) = -U_{1k}. \tag{11}$$

The space charge density in Eq. (10) is given by

$$\rho_1 = e(N_D^+ - N_A^- + p - n) = e(p_1 - p_0). \tag{12}$$

The hole concentration in region p_1 is obtained from

$$p_1 = p_0 \exp\left\{\frac{e\varphi_{1k}(z) - e\varphi_{1k}(a)}{kT}\right\}, \tag{13}$$

or

$$p_1 = p_k \exp\left\{\frac{e\varphi_{1k}(z)}{kT}\right\}. \tag{14}$$

The pre-exponential factor of Eq. (14) now can be rewritten as

$$p_k = p_0 \exp\left\{-\frac{e\varphi_{1k}(a)}{kT}\right\} = p_0 \exp\left\{\frac{eU_{1k}}{kT}\right\}. \tag{15}$$

leading to a differential equation

$$\frac{d^2\varphi_{1k}}{dz^2} = -\frac{ep_k}{\varepsilon_{fe}\varepsilon_0} \exp\left\{\frac{e\varphi_{1k}(z)}{kT}\right\} + \frac{ep_0}{\varepsilon_{fe}\varepsilon_0} \approx -\frac{ep_k}{\varepsilon_{fe}\varepsilon_0} \exp\left\{\frac{e\varphi_{1k}(z)}{kT}\right\}, \tag{16}$$

where ε_{fe} is the dielectric constant of the ferroelectric thin film. Integrating over region 1 we obtain

$$\varphi_{1k}(z) = -U_{1k} + \frac{kT}{e} \ln\left[1 + \tan^2\left(\frac{e(a-z)}{2kT}\sqrt{\frac{2p_k kT}{\varepsilon_{fe}\varepsilon_0}} \exp\left\{-\frac{eU_{1k}(z)}{kT}\right\}\right)\right]$$
$$= -U_{1k} + \frac{kT}{e} \ln\left[1 + \tan^2\left((a-z)\sqrt{\frac{e^2 p_0}{2\varepsilon_{fe}\varepsilon_0 kT}}\right)\right] = -U_{1k} + \frac{kT}{e} \ln\left[1 + \tan^2\left(\frac{a-z}{L}\right)\right], \tag{17}$$

where the characteristic length L is given by

$$L = \sqrt{\frac{2\varepsilon_{\rm fe}\varepsilon_0 kT}{e^2 p_0}}. \tag{18}$$

Finally, the potential and electric field distributions in the first region are given by

$$\varphi_1(z) = -U_{1k} + \frac{kT}{e}\ln\left[1+\tan^2\left(\frac{a-z}{L}\right)\right] + A + bP_{\rm S}z, \tag{19}$$

$$E_1 = -\frac{{\rm d}\varphi_1}{{\rm d}z} = \frac{kT}{eL}\tan\left(\frac{a-z}{L}\right) - bP_S. \tag{20}$$

A space charge may be formed in a ferroelectric thin film also by charge injection from metallic electrodes and trapping in the near electrode region.[23] In the case of electron trapping, the space charge density is determined by

$$\rho_1 = -eN_A^-, \tag{21}$$

resulting in an electric field of

$$E_1 = -\frac{{\rm d}\varphi_1}{{\rm d}z} = -eN_A^- z - bP_S. \tag{22}$$

The potential and electric field distributions in the second region are described by Eqs. (7) and (8), respectively.

In Fig. 1, the third and fourth regions form the ferroelectric–semiconductor contact. The potential distribution is obtained by solving the Poisson's Eq. (10) for $m=3$, 4 and the corresponding boundary conditions

$$\begin{cases} \varphi_3(z_1) = A + bP_S z_1 - U_k; & \left.\dfrac{{\rm d}\varphi_3}{{\rm d}z}\right|_{z=z_1} = bP_S \\ \varphi_4(z_2) = 0; & \left.\dfrac{{\rm d}\varphi_4}{{\rm d}z_2}\right|_{z=z_2} = 0 \end{cases}. \tag{23}$$

In the case of depletion, we use of the approximation

$$\begin{cases} \rho_3 = -ep_0 \quad (z_1 \le z \le l) \\ \rho_4 = en_0 \quad (l \le z \le z_2) \end{cases}. \tag{24}$$

Thus, the solutions of the Poisson equations are

$$\begin{cases} \varphi_3(z) = \dfrac{ep_0}{2\varepsilon_{\rm fe}\varepsilon_o}(z-z_1)^2 + A + bP_S z - U_k \\ \varphi_4(z) = -\dfrac{en_0}{2\varepsilon_{\rm sc}\varepsilon_o}(z-z_2)^2 \end{cases}, \tag{25}$$

and the electric field distributions in the third and fourth regions are given by

$$\begin{cases} E_3(z) = -\dfrac{{\rm d}\varphi_3(z)}{{\rm d}z} = -bP_{\rm S} - \dfrac{ep_0}{\varepsilon_1\varepsilon_0}(z-z_1) \\ E_4 = -\dfrac{{\rm d}\varphi_4(z)}{{\rm d}z} = \dfrac{en_0}{\varepsilon_2\varepsilon_0}(z-z_2) \end{cases}, \tag{26}$$

where $\varepsilon_{\rm sc}$ is the dielectric constant of the semiconductor.

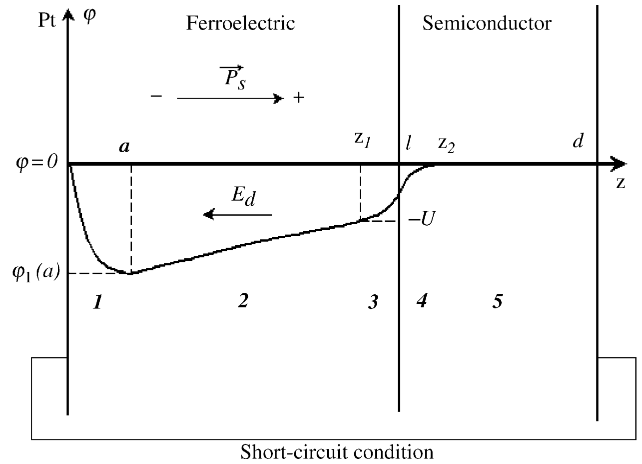

Fig. 2. The electric potential distribution in the metal–ferroelectric–semiconductor multilayer structure.

The thickness of space charge layers in the ferroelectric ($d_1 = l - z_1$) and the semiconductor ($d_2 = z_2 - l$) at the ferroelectric–semiconductor junction is determined by the boundary conditions at $z = l$

$$\begin{cases} D_3 = D_4 \\ \varphi_3 = \varphi_4 \end{cases} \tag{27}$$

where D is the electrical flux density, resulting in

$$\begin{cases} P_{\rm S}(1-\varepsilon_{\rm fe}\varepsilon_0 b) - ep_0(l-z_1) = -en_0(z_2-l) \\ A + bP_{\rm S}l - U_k + \dfrac{ep_0}{2\varepsilon_{\rm fe}\varepsilon_0}(l-z_1)^2 = -\dfrac{en_0}{2\varepsilon_{\rm sc}\varepsilon_0}(z_2-l)^2 \end{cases}. \tag{28}$$

Fig. 2 summarizes the electric potential distribution in the considered metal–ferroelectric–semiconductor multilayer structure.

3. LIMM of ferroelectric PZT (perovskite)–semiconducting PZT (fluorite) structures

We have fabricated PZT/SnO_2 and PZT/SiC ferroelectric–semiconductor heterojunctions by either depositing a SnO_2 thin film onto a PZT/Pt/SiO_2/Si substrate[24] or by depositing a PZT thin film on a SiC substrate heavily-doped by nitrogen.[25] However, in both cases a large density of interface states was present, and the pyroelectric current was very low. A pyroelectric current spectrum suitable for further analysis was obtained for (1 1 1) oriented ferroelectric PZT (perovskite)–semiconducting PZT (fluorite) structures deposited by sputtering.[13,26] The perovskite (300 nm)–fluorite (400 nm) heterostructure was fabricated by lowering the substrate temperature in a second step down to 450 °C. Details of the deposition process can be found elsewhere.[26,27] Low temperature deposited PZT thin films are known to contain excess lead of the form $Pb^{2+}Pb^{4+}O_3$ with a 4-valent Pb ion

on the B-site.[28,29] However, if a small part of B-site Pb^{4+} ions are reduced to Pb^{2+}, oxygen vacancies and mobile electrons appear forming a n-type semiconducting region in the fluorite sublayer. Indeed, the Seebeck coefficient was found to be negative, indicating a n-type conductor.

Film characterization by LIMM was described in detail in ref. 8. Briefly, we obtained the pyroelectric current spectrum generated by an semiconductor laser (LASER 2000, $\lambda = 1.55\ \mu$m, $P = 10$ mW) and modulated with frequencies up to 10 MHz. The pyroelectric current was transformed into a voltage by a I-U-converter (HCA-40 M, FEMTO Messtechnik GmbH, Berlin) and amplitude and phase are determined by an impedance-phase analyzer (SI1260, Solartron). The current spectra were corrected by reference measurements with an InGaAs photo-diode. The numerical reconstruction of the pyroelectric coefficient profile was based on a eight-layer thermal model. The profile reconstruction was performed using MATLAB software containing algorithms for the inverse solution of the appropriate Fredholm integral equation and a Tikhonov regularization method for stable numerical solutions.

The ferroelectric sublayer is similar to self-polarized (1 1 1) oriented PZT film deposited on platinized silicon wafers by reactive sputtering with well known properties.[8,14,20,27] These films comprise a space charge region with a thickness of about 240 nm near the bottom electrode.[30]

First, we consider a space charge formed by the mobile majority carriers. From a resistivity of our samples of $2.5 \times 10^{13}\ \Omega$ cm and a hole mobility of 1.2×10^{-6} cm^2/V s estimated by the extrapolation of high temperature data[15] to room temperature, we obtain a hole density of 2.1×10^{11} cm^{-3}. A direct extrapolation of the hole concentration to room temperature results in $n_h \approx 5 \times 10^{14}$ cm^{-3}. In the latter case, the contribution to the internal electric field is in order of 10^2 V/cm and may be neglected.

The depolarization field Eq. (8) is derived from the slope of the hysteresis curve $dE/dP|_{Ec} = 7.6 \times 10^9$ cm/F (cp,[13] Fig. 2). This is an upper limit from which the slope of the bulk ferroelectric hysteresis loop should be subtracted.[22] Thus, the depolarization field is $E_d \leq 2.3 \times 10^5$ V/cm for the considered sample of 900 nm thickness which is in the order of the coercive field of the initial self-polarized films $E_c = 1.3 \times 10^5$ V/cm. After a number of hysteresis cycles the coercive field lowers to 6×10^4 V/cm. Following[17] we have also determined the reciprocal capacitance of the non-ferroelectric interface layer $d_i/\varepsilon_i\varepsilon_0 = 3.8 \times 10^5$ cm^2/F from the thickness dependence of perovskite PZT films. This value denotes a larger contribution of interface states to film properties compared to annealed films deposited by MOCVD ($d_i/\varepsilon_i\varepsilon_0 = 5 \times 10^4$ cm^2/F[17]), CSD deposited films ($d_i/\varepsilon_i\varepsilon_0 = 7.54 \times 10^4$ cm^2/F[31]), and sputtered PZT films with $SrRuO_3$ electrodes ($d_i/\varepsilon_i\varepsilon_0 \approx 10^3$ cm^2/F[31]). The depolarization factor is in our case $b = d_i/\varepsilon_i\varepsilon_0 d = 4.22 \times 10^9$ cm/F in agreement with the value obtained from the hysteresis slope. The dielectric constant of the perovskite bulk amounts to $\varepsilon_{fe} = 400$. The value of the fluorite sublayer

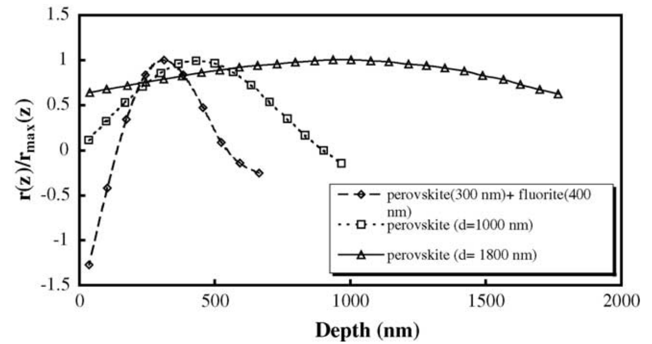

Fig. 3. Reconstructed from LIMM measurements pyroelectric response function profiles of ferroelectric PZT thin films in comparison with a ferroelectric semiconductor PZT structure. The depth is counted from the film surface.

was determined from the series connection of capacitances as $\varepsilon_{sc} \approx 17$.

Fig. 3 compares the pyroelectric coefficient profile of perovskite PZT thin films with a thickness of 900 nm and 1800 nm, respectively, compared with the profile of a 300 nm perovskite PZT/400 nm fluorite PZT structure. The algorithm for solving Eq. (1) using the Tikhonov regularisation method is described in detail in.[8]

With increasing thickness, the profile of ferroelectric thin films becomes smoother due to a decreasing according to Eq. (8) depolarization field. The internal electric field near the bottom electrode was estimated for the 1000 nm thick sample as about 2×10^5 V/cm. This explains in part the negative value of $r(z)$ in this case. The negative value of the pyroelectric response function in the semiconductor region of the ferroelectric semiconductor structure is probably an reconstruction artifact. In fact, we have previously shown that smooth profiles were reconstructed using an appropriate thermal multilayer model within an uncertainty of 2–3% in dependence on the discretization approach.[32] On the other hand, the uncertainty of the reconstruction of a Dirac-pulse-like polarization profile exceeds 90%. Therefore, profiles containing discontinuities, for instance at interfaces, are not well reconstructed.

4. Conclusions

In this work, the LIMM problem of a multilayer structure consisting of layers with ferroelectric polarization, with both ferroelectric and space charge induced polarization, and with solely space charge induced polarization was considered. The problem was reduced to the calculation of the internal electric field. We have shown that in the case of a metal–ferroelectric–semiconductor structure—Pt–ferroelectric PZT (perovskite)–semiconducting PZT (fluorite) the internal electric field is dominated by the depolarization field generated by the non-ferroelectric interface layer at the bottom electrode. New algorithms of profiles reconstruction from LIMM data are required for

specimens containing interfaces, steep polarization gradients and polarization discontinuities.

Acknowledgements

This work was supported by the German Research Council (Deutsche Forschungsgemeinschaft) as part of the Research Group FOR520 and by the Herbert Quandt Foundation. The authors thank T. Sandner for the measurement of the pyroelectric current spectrum and the reconstruction of the pyroelectric response function.

References

1. Lang, S. B. and Das-Gupta, D. K., Laser-intensity-modulation method: a technique for determination of spatial distributions of polarization and space charge in polymer electrets. *J. Appl. Phys.*, 1986, **59**, 2151–2160.
2. Collins, R. E., Analysis of spatial distribution of charges and dipoles in electrets by a transient heating technique. *J. Appl. Phys.*, 1976, **47**, 4804–4808.
3. Chynoweth, A. G., Dynamic method for measuring the pyroelectric effect with special reference to barium titanate. *J. Appl. Phys.*, 1956, **27**, 78–84.
4. Bezdetny, N. M., Zeinally, A. Kh. and Khutorsky, V. E., Investigation of the polarization distribution in ferroelectrics by a dynamic pyroeffect method (in Russian). *Izv. AN SSSR Ser. Fiz.*, 1984, **48**, 200–203.
5. Bloss, B., Emmerich, R. and Bauer, S., Thermal wave probing of pyroelectric distributions in the surface region of ferroelectric materials: a new method of analysis. *J. Appl. Phys.*, 1992, **72**, 5363–5370.
6. Lang, S. B., New theoretical analysis for the laser intensity modulation method (LIMM). *Ferroelectrics*, 1990, **106**, 269–274.
7. Glinchuk, M. D., Eliseev, E. A., Deineka, A., Jastrabik, L., Suchaneck, G., Sandner, T., Gerlach, G. and Hrabovsky, M., Polarization and refractive index profiles of ferroelectric thin films. *Integr. Ferroelectr.*, 2001, **38**, 101–110.
8. Sandner, T., Suchaneck, G., Koehler, R., Suchaneck, A. and Gerlach, G., High frequency LIMM—a powerful tool for ferroelectric thin film characterization. *Integr. Ferroelectr.*, 2002, **46**, 243–257.
9. Känzig, W., Space charge layer near the surface of a ferroelectric. *Phys. Rev.*, 1955, **98**, 549–550.
10. Mehta, R. R., Silverman, B. D. and Jacobs, J. T., Depolarization fields in thin ferroelectric films. *J. Appl. Phys.*, 1973, **44**, 3379–3385.
11. Lur'e, M. S., Vasil'eva, E. I. and Ignat'eva, I. V., Ferroelectric films with a square hysteresis loop. *Izv. AN SSSR Ser. Fiz.*, 1960, **24**, 1376–1379.
12. Zook, J. D. and Liu, S. T., Pyroelectric effect in thin film. *J. Appl. Phys.*, 1978, **49**, 4604–4606.
13. Suchaneck, G., Solnyshkin, A.V., Suchaneck, A. and Gerlach, G., Polarization profiling of metal–ferroelectric–semiconductor structures by LIMM. This volume.
14. Suchaneck, G., Deyneka, A., Jastrabik, L. and Gerlach, G., Stability of space charge compensated ferroelectrics. *Integr. Ferroelectr.*, 2004, in press.
15. Prisedsky, V. V., Shishkovsky, V. I. and Klimov, V. V., High-temperature electrical conductivity and point defects in lead zirconate-titanate. *Ferroelectrics*, 1978, **17**, 465–468.
16. Kretschmer, R. and Binder, K., Surface effects on phase transitions in ferroelectrics and dipolar magnets. *Phys. Rev.*, 1978, **B20**, 1065–1076.
17. Larsen, P. K., Dormans, G. J. M., Taylor, D. J. and van Veldhoven, P. J., Ferroelectric properties and fatigue of $PbZr_{0.51}Ti_{0.49}O_3$ thin films of varying thickness: blocking layer model. *J. Appl. Phys.*, 1994, **76**, 2405–2413.
18. Bell, J. M. and Knight, P. C., Ferroelectric electrode interaction of $BaTiO_3$ and PZT thin films. *Integr. Ferroelectr.*, 1994, **4**, 325–332.
19. Lee, J. J., Thio, C. L. and Desu, S. B., Electrode contacts on ferroelectric $Pb(Zr_xTi_{1-x})O_3$ and $SrBi_2Ta_2O_9$ thin films and their influence on fatigue properties. *J. Appl. Phys.*, 1995, **78**, 5073–5078.
20. Suchaneck, G., Gerlach, G., Poplavko, Yu., Kosarev, A. I. and Andronov, A. N., Self-polarization mechanism in textured pyroelectric $Pb(Ti_{1-x}Zr_x)O_3$ films. *Mater. Res. Symp. Proc.*, 2001, **655**, C.C.7.7.1–C.C.7.7.6.
21. Sakashita, Y., Segawa, H., Tominaga, K. and Okada, M., Dependence of electrical properties on film thickness in $(Pb(Zr_xTi_{1-x})O_3$ thin films produced by metalorganic chemical vapor deposition. *J. Appl. Phys.*, 1993, **73**, 7857–7863.
22. Tagantsev, A. K., Landivar, M., Colla, E. and Setter, N., Identification of passive layer in ferroelectric thin films from their switching parameters. *J. Appl. Phys.*, 1995, **78**, 2623–2630.
23. Cillessen, J. F. M., Prins, M. W. J. and Wolf, R. M., Thickness dependence of switching voltage in all-oxide ferroelectric thin-film capacitors prepared by pulsed laser deposition. *J. Appl. Phys.*, 1997, **81**, 2777–2783.
24. Afanasjev, V. P., Pankrashkin, A. V., Kramar, G. P., Suchaneck, G. and Gerlach, G., Powerless light dosimeters based on charge storage at semiconductor-ferroelectric interfaces. In *Eurosensors XVI, 16th European Conference on Solid-State Transducers*, 2002, pp. 709–710.
25. Suchaneck, G. and Gerlach, G., Image capture sensors based on charge storage at semiconductor-ferroelectric interfaces. *Integr. Ferroelectr.*, 2003, **54**, 619–629.
26. Lin, W.-M., Koehler, R., Suchaneck, G., Sandner, T., Gerlach, G., Bruchhaus, R., Wersing, W., Deineka, A. and Jastrabik, L., Self-polarization profile of RF-sputtered PZT thin films.. In *Proceedings of Materials Week 2000, International Congress on Advanced Materials, their Processes and Application*, 2000., www.materialsweek.org/proceedings/.
27. Bruchhaus, R., Pitzer, D., Primig, R., Wersing, W. and Xu, Y., Deposition of self-polarized PZT films by planar multi-target sputtering. *Integr. Ferroelectr.*, 1997, **14**, 141–149.
28. Muralt, P., Hiboux, S., Mueller, C., Maeder, T., Sagalowicz, L., Egami, T. and Setter, N., Excess lead in the perovskite lattice of PZT thin film made by in-situ reactive sputtering. *Integr. Ferroelectr.*, 2001, **36**, 53–62.
29. Mandeljc, M., Maltic, B. and Kosec, M., Where is PbO excess in CSD PZT thin films crystallized at 400 °C?. In *Processing of Electroceramics Symposium 2003*, 2003., www.polecer.rwth-aachen.de/Bled.Poster.Mandeljc.jpg.
30. Lu, X., Schlaphof, F., Grafström, S., Loppacher, C., Eng, L. M., Suchaneck, G. and Gerlach, G., Scanning force microscopy investigation of the $Pb(Zr_{0.25}Ti_{0.75})O_3$/Pt interface. *Appl. Phys. Lett.*, 2002, **81**, 3215–3217.
31. Ellerkmann, U., Schorn, P., Bolten, D., Boettiger, U., Waser, R., Bruchhaus, R. and Yamakawa, K., Influence of asymmetric oxide electrode structures on the interface capacity and failure mechanism in PZT thin films. *Integr. Ferroelectr.*, 2003, **52**, 63–71.
32. Gerlach, G., Sandner, T. and Suchaneck, G., Determination of polarization profiles inside ferroelectric thin films using the laser intensity modulation method. In *Proceedings of SPIE on Testing, Reliability, and Application of Micro and Nano-Material Systems, Vol 5054*, ed. N. Meyendorf, G.Y. Baaklini and B. Michel, SPIE, Bellingham, WA, 2003, pp.157–171.